SEMARAK ILMU PUBLISHING

Journal of Advanced Research in Fluid Mechanics and Thermal Sciences

Journal homepage:
https://semarakilmu.com.my/journals/index.php/fluid_mechanics_thermal_sciences/index
ISSN: 2289-7879

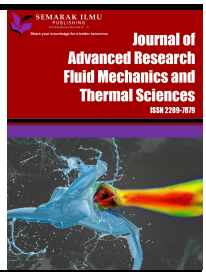

Stability analysis of Joule heating and viscous dissipation effects on micropolar nanofluid flow over nonlinear stretching/shrinking surface

Khuram Rafique[1], Tatheer Fatima[2], Gamal Elkahlout[3,*]

[1] Centre of Excellence for Social Innovation and Sustainability, Institute of Engineering Mathematics, University Malaysia Perlis, Arau, Perlis, Malaysia
[2] Department of Mathematics, University of Sialkot, Pakistan
[3] School of Business Studies, Arab Open University, Riyadh, Saudi Arabia

ARTICLE INFO

Article history:
Received 8 July 2025
Received in revised form 29 January 2026
Accepted 16 February 2026
Available online 28 February 2026

Keywords:
micropolar nanofluid; Joule heating; viscous dissipation; stretching/shrinking surface; stability analysis; BVP4C.

ABSTRACT

In these days, due to the demand of compact systems the heat dissipation rate is subject under discussion. Water cooling systems and air cooling systems are not that much suitable in tiny systems sue to their structure. Therefore, using of nanofluids for heating and cooling is preferred in industries, and by minimizing the structure of the system, cost may also be minimized. By increasing the rate of energy transmission, nanoliquids aids in strengthen the performance of thermal systems. Nanoliquids are widely employed in many different applications including gasoline, automotive coolant and medical and electrical equipment to lower heat resistance. In view of these applications, the main goal of this research is to study the energy and mass transmission of micropolar nanofluid flow through a vertical surface by incorporating viscous dissipation and Joule heating effects. The flow model converted into nonlinear ODE's via similarity variables. Furthermore triple solutions are derived via MATLAB BVP4C package. Moreover, examination is performed to evaluate their stability. The investigation showed that only first result is stable remaining two are unstable. The results reported that the temperature distribution shows increasing behavior for the increment in Eckert number. While the velocity of the liquid slow down on the increment in magnetic strength. In the same vein the temperature distribution decreases for the increment in Brownian factor.

1. Introduction

The investigation of energy transmission for the boundary layer flow over a stretching/shrinking surface has generated an extensive importance worldwide, since it has many engineering and industrial applications, for instance, paper production, hot rolling, glass-fiber production, etc. [1-2]. Recently, due to the advancement in nanotechnology nanofluid has gained intension of the current researchers. Nanotechnology has wide use as nanomedicine in the medical field. Few nanoparticles have possible utilization in targeted medicinal products, novel diagnostic instruments, pharmaceutical products and tissue engineering. Moreover, heat transfer ability of nanofluid is

* *Corresponding author.*
E-mail address: g.elkahlout@arabou.edu.sa

https://doi.org/10.37934/arfmts.138.1.114

almost better than the regular liquid because of its thermophysical characteristics. In view of this ability, researchers have utilized this energy transfer liquid in practical uses.

Nanofluid has utilized in several real life uses including vehicle radiators, refrigerators, cooling systems, thermal energy storage system etc. Nanofluid is comprised by mixing nanometer-size particles in regular liquid [3]. The numerical treatment for bio-convection of nanoliquid was examined by [4]. Recently, shape characteristics effect on the flow phenomenon of nanoliquid was studied by [5]. Furthermore, investigation of thermal analysis for nanoliquid flow on a sphere was examined by [6]. Further, [7] probed nanoliquid flow phenomenon for thermal analysis through a vertical cylinder.

Also, the numerical investigation by taking ternary nanoparticles for rotatry flow was discussed by [8]. The effect of nanofluid stability on thermal efficiency has been investigated by [9]. Dual solution for hybrid nanoliquid via stability analysis was obtained by [10]. Analysis of energy and mass transmission for the flow of nanofluid by incorporating radiations was studied [11].

Soret and Dufour play significant role in the real life applications. A mass flux caused by change in temperature known Soret effect which is referred as thermal diffusion. While energy flux cause by change in concentration called Dufour effect. Soret and Dufour effects are very important for the applications in industrial processes, geothermal energy, petroleum reservoirs etc.

The numerical investigation of nanoliquid with the impact of the Soret and Dufour was analysed [12]. For nonlinear extendable surface with Soret and Dufour's impacts the flow of Casson nanoliquid was conducted [13]. Further Soret Dufour effect was along with chemical reaction investigated [14]. Soret and Dufour impacts by incorporating multiple slip effects through a flexible surface was examined [15]. Moreover, a Soret and Dufour impact on MHD mixed convection through extending/shrinking surfaces was calculated [16]. Three dimensional rotating flow of nanoliquid with Soret Dufour effects was examined [17]. Soret and Dufour impacts on a flow across a vertical plate in a porous medium were discussed [18].

MHD is an essential part of engineering applications and natural phenomena; it defines the contact among electrically conducting liquids and magnetic fields. In real life magnetic field occurs everywhere in the nature which indicates that MHD properties available under the presence of electrically conducting liquids in natural phenomenon. It has many application for instance, in space weather, plasma physics, and in power plants etc.

MHD helps us to improve our knowledge for plasmas and their performances in various atmospheres. Thermal analysis of electrically conducting fluid flow of nanoliquid by incorporating Joule heating was studied [19]. Further, [20] examined nanoliquid flow phenomenon with magnetic field effect numerically. Moreover, the numerical treatment of magnetized nanoliquid flow for a flexible surface was discussed by [21]. In the same vein [22] studied that magnetic field impacts are very useful for x-ray, ultrasound and many electric vehicles. Whereas, the dual solution of nanoliquid flow phenomenon with magnetic effects was examined by [23].

The role of viscous dissipation in boundary layer flow phenomenon for industrial applications is remarkable due to which it becomes hot area of research. It has many applications in heat transmission for instance apparatus chilling, internal freezer and chiller. The numerical investigation viscous dissipation on hybrid nanoliquid was examined by [24]. Recently, [25] examined the viscous dissipation impact on the nanoliquid flow phenomenon for a vertical cone numerically. Furthermore, for nonhomogeneous nanoliquid flow phenomenon with viscous dissipation for stagnation flow was examined by [26].

The main aim of this research is to analyze the impact of Joule heating and viscous dissipation on micropolar nanoliquid flow through a vertical surface. This study has many uses in energy transmission such as internal freezer and chiller, vehicle thermal controlling, curative progressions

and firewood cells. The primary goals of this investigation are to evaluate the multifaceted physical significance of key flow parameters including thermal radiation and Dufour impacts, viscous dissipation, Joule heating and porosity through detailed graphical analysis. Furthermore, the stability analysis for multiple solutions of micro-rotational nanofluid flow with Brownian motion, thermophoretic effects, Joule heating and viscous dissipation through permeable vertical surface offers novel insights. In view of author best knowledge there is no study conducted to find the triple solution for micropolar nanofluid flow with Joule heat and viscous dissipation impacts. Therefore, in order to fill this research gap this study has been conducted.

Moreover, the utilization of Soret and Dufour impacts play a key role in practical applications including nuclear reactors, production of plastic sheet, cooling electronic devices, polymer manufacture and ceramics. Whereas, for various technology systems a high temperature required which can be possible with thermal radiations, thus thermal radiations are uses in solar systems, electric devices and in exploration of space missions.

The rest of the article is organized as; in the next part 2, the problem formulation is provided. In part 3, we provide the detail of stability analysis. In part 4, we discussed the numerical and graphical results. The main finding of this research work is presented in the part 5.

2. Problem Formulation

An incompressible Micropolar nanofluid flow over a vertical surface by incorporating Joule heating and viscous dissipation is considered. The stretching/shrinking sheet is supposed to have velocity $u_w(x) = ax^m$, with variable surface temperature $T_w(x) = T_\infty + bx^{2m-1}$ along with wall concentration $C_w(x) = C_\infty + cx^{2m-1}$, where a, b, c are constants. The magnetic field is taken an inclined to the surface. Further, thermal radiation effects are considered in this study. The flow model with coordinate system is presented in Figure 1. The limitations and assumptions in this study are

- The vertical surface is porous.
- g represents the gravitational acceleration.
- B_0 is taken as magnetic field strength.
- Soret effect and viscous dissipation incorporated in energy equation.
- Dufour impact incorporated in mass equation.

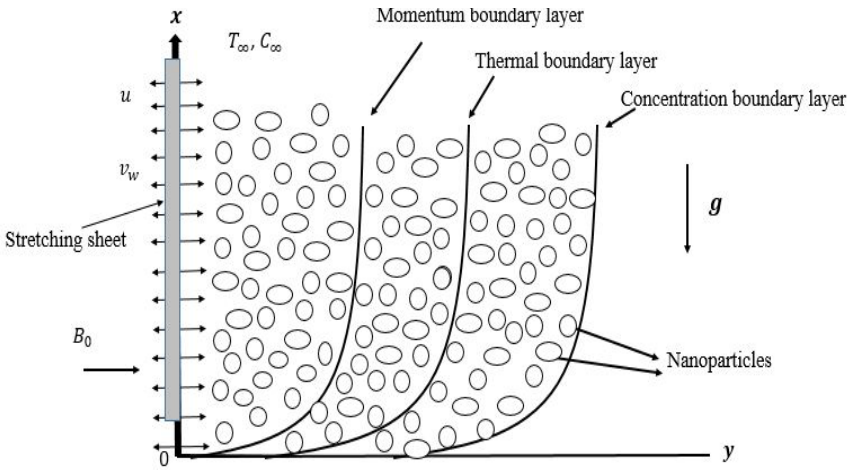

Fig. 1 Flow structure with coordinate system

The flow equations in view of above mentioned asumptions can be expressed in the form.

$$\nabla . V = 0, \tag{a}$$

$$\rho \frac{dV}{dt} = (\mu + k)\nabla^2 V + k\nabla N - \sigma B^2 cos\gamma V + g[\,\beta_T(T - T_\infty) + \beta_C(C - C_\infty)], \tag{b}$$

$$\rho j \frac{dN}{dt} = \gamma \nabla^2 N - k(2N - \nabla \times V), \tag{c}$$

$$\rho c_p \frac{dT}{dt} = (k)\nabla^2 T + \frac{\partial q_r}{\partial y} + \left(\rho c_p\right)[D_B \nabla C . \nabla T + \frac{D_T}{T_\infty}(\nabla T)^2] - \frac{D_m K_T}{C_s} \nabla^2 C + \sigma B^2 cos\gamma u^2 \tag{d}$$

$$\frac{dC}{dt} = D_B \nabla^2 C + \frac{D_T}{T_\infty} \nabla^2 T + \frac{D_m K_T}{T_m} \nabla^2 T, \tag{e}$$

In view of [27, 28] above model converted into

$$\frac{\partial u}{\partial x} + \frac{\partial v}{\partial y} = 0 \tag{1}$$

$$\rho\left(u\frac{\partial u}{\partial x} + v\frac{\partial u}{\partial y}\right) = (\mu + k)\frac{\partial^2 u}{\partial y^2} + k\frac{\partial N}{\partial y} - \sigma B^2 cos\gamma u + \rho g[\,\beta_T(T - T_\infty) + \beta_C(C - C_\infty)] \tag{2}$$

$$u\frac{\partial N}{\partial x} + v\frac{\partial N}{\partial y} = \frac{1}{\rho_j}\left[\gamma\frac{\partial^2 N}{\partial y^2} - k\left(2N + \frac{\partial u}{\partial y}\right)\right] \tag{3}$$

$$u\frac{\partial T}{\partial x} + v\frac{\partial T}{\partial y} = \left(\alpha + \frac{16\sigma^* {T_\infty}^3}{3k^*\rho C_p}\right)\frac{\partial^2 T}{\partial y^2} + \left(\frac{(\mu+k)}{\rho C_p}\right)\left(\frac{\partial u}{\partial y}\right)^2 + \tau_w\left[D_B\frac{\partial C}{\partial y}\frac{\partial T}{\partial y} + \frac{D_T}{T_\infty}\left(\frac{\partial T}{\partial y}\right)^2\right] - \frac{D_m K_T}{C_s C_p}\frac{\partial^2 C}{\partial y^2} + \frac{\sigma B^2}{\rho C_p} cos\gamma u^2 \tag{4}$$

$$u\frac{\partial C}{\partial x} + v\frac{\partial C}{\partial y} = D_B\frac{\partial^2 C}{\partial y^2} + \frac{D_T}{T_\infty}\frac{\partial^2 T}{\partial y^2} + \frac{D_m K_T}{T_m}\frac{\partial^2 T}{\partial y^2} \tag{5}$$

Subject to boundary conditions

$$\begin{aligned} &v = v_w;\ u = \lambda u_w(x);\ N = -n\frac{\partial u}{\partial y};\ T = T_w; C = C_w \quad \text{at} \quad y = 0 \\ &u \to 0\ ;\ v \to 0\ ;\ N \to 0\ ;\ T \to T_\infty\ ;\ C \to C_\infty \qquad \text{at} \quad y \to \infty \end{aligned} \tag{6}$$

Where u and v represents the velocity coefficients along the x-axis and y-axis, respectively. While $\rho, k, j, N, \nu, \gamma$ are density, vortex viscosity, micro-inertia density, angular velocity, kinematic viscosity, spin gradient viscosity, respectively. K^*, σ^* mean absorption factor, and Stefan-Boltzmann constant, respectively. D_m, D_B, D_T, T_m, K_T show the mass diffusivity, Brownian motion, thermophoresis diffusion, fluid mean temperature, thermal diffusion ratio parameter. Whereas, λ is stretching/shrinking factor where $\lambda < 0$ denotes a surface that is shrinking while $\lambda > 0$ denotes a surface that is expand. The similarity variables utilized for this research are given as.

$$u = ax^m f'\ ,\ \ v = -\sqrt{\frac{(m+1)\nu a}{2x^{m+1}}}\ x^m f - yf'\ \frac{ax^{m-1}}{2}(m-1)\ ,\ \ \eta = y\sqrt{\frac{(m+1)ax^{m-1}}{2\nu}},$$

$$N = \ ax^m\sqrt{\frac{a(m+1)x^{m-1}}{2\nu}}\ h(\eta)\ ,\ \ \theta(\eta) = \frac{(T-T_\infty)}{(T_w-T_\infty)}$$

The following ODEs are obtained by utilizing the similarity variable from Eq. (1) to Eq. (5).

$$(1+K)f''' + Kh' + ff'' + \left(\frac{2}{m+1}\right)(Gr\,\theta + Gc\,\phi) - \left(\frac{2m}{m+1}\right)f'^2 - \left(\frac{2M}{m+1}\right)cos\gamma f' = 0 \quad (8)$$

$$\left(1+\frac{K}{2}\right)h'' + fh' - \left(\frac{3m-1}{m+1}\right)hf' - \left(\frac{2K}{m+1}\right)(2h+f'') = 0 \quad (9)$$

$$\frac{1}{Pr}\left(1+\frac{4}{3}Rd\right)\theta'' + Nb\,\theta'\phi' + Nt\,\theta'^2 + EcMf'cos\gamma + \theta' f - Df\,\phi'' + (1+k)Ecf''^2 = 0 \quad (10)$$

$$\phi'' + \frac{Nt}{Nb}\theta'' + Sr\,Sc\,\theta'' + \phi' f\,Sc = 0 \quad (11)$$

Here, primes represent the differentiation with respect to η.

$$\alpha = \frac{k}{\rho C_p},\ M = \frac{\sigma B_0^2}{\rho a},\ Nb = \frac{\tau_w D_B (C_w - C_\infty)}{\nu},\ K = \frac{k}{\nu},\ Rd = \frac{4\sigma^* T_\infty^3}{kK^*},\ Gr = \frac{Gr_x}{Re_x^2},\ Pr = \frac{\nu}{a},\ Sc = \frac{\nu}{D_B}$$

The associative boundary conditions take the form:

$$f(0) = f_w,\ f'(0) = \lambda,\ h(\eta) = -nf''(\eta),\quad \theta(\eta) = 1,\quad \phi(\eta) = 1;\ f'(\eta) \to 0,$$

$$h(\eta) \to 0,\ \theta(0) \to 0,\ \phi(0) \to 0 \quad \text{as } \eta \to \infty \quad (12)$$

Here, $v_w = -\sqrt{\frac{a\nu(m+1)}{2}}\,x^{\left(\frac{m-1}{2}\right)}$ denotes suction factor, $f_w > 0$ for suction. For the current problem, Nusselt, Sherwood number, and skin friction given as follows:

$$Nu_x = \frac{xq_w}{k(T_w - T_\infty)}, Sh_x = \frac{xq_m}{D_B(C_w - C_\infty)},\ C_f = \frac{\tau_w}{u_{w^2}\rho} \quad (13)$$

When,

$$q_w = -\left(k + \frac{16\sigma^* T_\infty^3}{3k^*}\right)\frac{\partial T}{\partial y}\ ,\ q_m = -D_B\frac{\partial C}{\partial y}, \text{ and } \quad \tau_w = (\mu + k)\frac{\partial u}{\partial y} + kN \quad (14)$$

The relevant skin friction factor is $C_{fx} = (1 + (1-m)K)f''(0)$, local Nusselt number $-\theta'(0)$, and the Sherwood number is $-\phi'$ become in the form

$$-\theta'(0) = \frac{Nu_x}{\left(1+\frac{4}{3}Rd\right)\sqrt{\frac{m+1}{2}Re_x}},\ -\phi'(0) = \frac{Sh_x}{\sqrt{\frac{m+1}{2}Re_x}},\quad C_{fx}(0) = C_f\sqrt{\frac{2}{m+1}Re_x} \quad (15)$$

Where, $Re_x = \frac{u_w x}{\nu}$.

3. Stability Analysis

In this research work, more than one solution was found; therefore, in order to find a stable solution, a Stability analysis is performed. For finding a stable solution via stability analysis, first of all, it is necessary to convert the flow model into an unsteady flow, for which we introduce a new variable τ. Therefore, a new form of the flow model in unsteady form is

$$\rho\left(\frac{\partial u}{\partial t} + u\frac{\partial u}{\partial x} + v\frac{\partial u}{\partial y}\right) = (\mu + k)\frac{\partial^2 u}{\partial y^2} + k\frac{\partial N}{\partial y} - \sigma B^2 cos\gamma u + \rho g[\,\beta_T(T - T_\infty) + \beta_C(C - C_\infty)] \quad (16)$$

$$\left(\frac{\partial N}{\partial t} + u\frac{\partial N}{\partial x} + v\frac{\partial N}{\partial y}\right) = \frac{1}{\rho_j}\left[\gamma\frac{\partial^2 N}{\partial y^2} - k\left(2N + \frac{\partial u}{\partial y}\right)\right] \quad (17)$$

$$\left(\frac{\partial T}{\partial t}+u\frac{\partial T}{\partial x}+v\frac{\partial T}{\partial y}\right)=\left(\alpha+\frac{16\sigma^{*}{T_{\infty}}^{3}}{3k^{*}\rho C_{p}}\right)\frac{\partial^{2}T}{\partial y^{2}}+\left(\frac{(\mu+k)}{\rho C_{p}}\right)\left(\frac{\partial u}{\partial y}\right)^{2}+\tau_{w}\left[D_{B}\frac{\partial C}{\partial y}\frac{\partial T}{\partial y}+\frac{D_{T}}{T_{\infty}}\left(\frac{\partial T}{\partial y}\right)^{2}\right]-\frac{D_{m}K_{T}}{C_{s}C_{p}}\frac{\partial^{2}C}{\partial y^{2}}+\frac{\sigma B^{2}}{\rho C_{p}}cos\gamma u^{2} \quad (18)$$

$$\left(\frac{\partial C}{\partial t}+u\frac{\partial C}{\partial x}+v\frac{\partial C}{\partial y}\right)=D_{B}\frac{\partial^{2}C}{\partial y^{2}}+\frac{D_{T}}{T_{\infty}}\frac{\partial^{2}T}{\partial y^{2}}+\frac{D_{m}K_{T}}{T_{m}}\frac{\partial^{2}T}{\partial y^{2}} \quad (19)$$

The following are the new similarity parameters that have been presented:

$$u=ax^{m}\frac{\partial f(\eta,\tau)}{\partial\eta},\ v=-\sqrt{\frac{(m+1)va}{2x^{m+1}}}\,x^{m}f(\eta,\tau)-y\frac{\partial f(\eta,\tau)}{\partial\eta}\frac{ax^{m-1}}{2}(m-1)$$
$$\eta=y\sqrt{\frac{(m+1)ax^{m-1}}{2v}},\ \tau=ax^{m-1}t,\ N=ax^{m}\sqrt{\frac{a(m+1)x^{m-1}}{2v}}\,h(\eta,\tau),$$
$$\theta(\eta,\tau)=\frac{(T-T_{\infty})}{(T_{w}-T_{\infty})},\ \phi(\eta,\tau)=\frac{(C-C_{\infty})}{(C_{w}-C_{\infty})}, \quad (20)$$

Eq. (16) to Eq. (19) are used to obtain it by using Eq. (20).

$$(1+K)\frac{\partial^{3}f}{\partial\eta^{3}}+K\frac{\partial h}{\partial\eta}+f\frac{\partial^{2}f}{\partial\eta^{2}}+\frac{2}{m+1}(Gr\,\theta+Gc\,\phi)-\frac{2}{m+1}\frac{\partial^{2}f}{\partial\eta\partial\tau}-\frac{2m}{m+1}\left(\frac{\partial f}{\partial\eta}\right)^{2}-\frac{2M}{m+1}cos\gamma\frac{\partial f}{\partial\eta}=0 \quad (21)$$

$$\left(1+\frac{K}{2}\right)\frac{\partial^{2}h}{\partial\eta^{2}}+f\frac{\partial h}{\partial\tau}-\left(\frac{3m-1}{m+1}\right)h\frac{\partial f}{\partial\eta}-\frac{2K}{m+1}\left(2h+\frac{\partial^{2}f}{\partial\eta^{2}}\right)-\frac{2}{m+1}\frac{\partial h}{\partial\tau}=0 \quad (22)$$

$$\frac{1}{Pr}\left(1+\frac{4}{3}Rd\right)\frac{\partial^{2}\theta}{\partial\eta^{2}}+Nb\frac{\partial\theta}{\partial\eta}\frac{\partial\phi}{\partial\eta}+Nt\left(\frac{\partial\theta}{\partial\eta}\right)^{2}-\frac{2}{(m+1)}\frac{\partial\theta}{\partial\tau}+EcM\left(\frac{\partial f}{\partial\eta}\right)^{2}cos\gamma+f\frac{\partial\theta}{\partial\eta}+-Df\frac{\partial^{2}\phi}{\partial\eta^{2}}+Ec(1+K)\left(\frac{\partial^{2}f}{\partial\eta^{2}}\right)^{2}=0 \quad (23)$$

$$\frac{\partial^{2}\phi}{\partial\eta^{2}}+\frac{\partial\phi}{\partial\eta}f\,Sc+\frac{Nt}{Nb}\frac{\partial^{2}\theta}{\partial\eta^{2}}-\frac{2}{m+1}\frac{\partial\phi}{\partial\tau}Sc+Sr\,Sc\,\frac{\partial^{2}\theta}{\partial\eta^{2}}=0 \quad (24)$$

Subjected to boundary settings

$$f(0,\tau)=f_{w},\ \frac{\partial f(0,\tau)}{\partial\eta}=\lambda,\ h(0,\tau)=-n\frac{\partial^{2}f(0,\tau)}{\partial\eta^{2}},\ \theta(0,\tau)=1,\ \phi(0,\tau)=1$$
$$\frac{\partial f(\eta,\tau)}{\partial\eta}\to 0,h(\eta,\tau)\to 0,\theta(\eta,\tau)\to 0,\phi(\eta,\tau)\to 0\qquad as\ \eta\to\infty \quad (25)$$

The perturbation function's goal is to investigate any possible disturbances in the solutions.

$$f(\eta)=f_{0}(\eta),h(\eta)=h_{0}(\eta),\theta(\eta)=\theta_{0}(\eta),\phi(\eta)=\phi_{0}(\eta)$$
$$f(\eta,\tau)=f_{0}(\eta)+e^{-\varepsilon\tau}F(\eta)$$
$$h(\eta,\tau)=h_{0}(\eta)+e^{-\varepsilon\tau}H(\eta)$$
$$\theta(\eta,\tau)=\theta_{0}(\eta)+e^{-\varepsilon\tau}G(\eta)$$
$$\phi(\eta,\tau)=\phi_{0}(\eta)+e^{-\varepsilon\tau}S(\eta) \quad (26)$$

Where smallest eigenvalue is ε and $F(\eta)$, $H(\eta,\ G(\eta),\ S(\eta)$are small relative to $f_{0}(\eta)$, $h_{0}(\eta)$, $\theta_{0}(\eta)$, $\phi_{0}(\eta)$ respectively. Eq. (26) is used to create the linearized eigenvalue equations for Eq. (21) to Eq. (24), which generate the following:

$$(1+K)F_{0}'''+KH_{0}'-\left(\frac{2}{(m+1)}\right)F_{0}'\left[M-\varepsilon-2mf_{0}'\right]+\left(\frac{2}{(m+1)}\right)\left[GrG_{0}+Gc\,S_{0}\right]+f_{0}F_{0}''+Ff_{0}''=0 \quad (27)$$

$$\left(1+\frac{K}{2}\right)H_0'' - \frac{2}{(m+1)}H_0(2K-\varepsilon) - \frac{2K}{(m+1)}F_0'' + f_0H_0' + F_0h_0' - \left(\frac{3m-1}{m+1}\right)[H_0f_0' + h_0F_0'] = 0 \quad (28)$$

$$\frac{1}{Pr}\left(1+\frac{4}{3}Rd\right)G_0'' + \theta_0'[Nb\,S_0' + Nt\,2G_0' + F_0] + G_0'[Nb\,\phi_0' + f_0] + \varepsilon G_0 + 2EcM\cos\gamma f_0'F_0' - Df\,S_0'' + Ec(1+K)f_0''F_0'' = 0 \quad (29)$$

$$S_0'' + G_0''\left[\frac{Nt}{Nb} + Sr\,Sc\right] + Sc\,\varepsilon S_0 + \phi_0'F_0 + S_0'f_0 = 0 \quad (30)$$

With boundary conditions:

$$F_0(0) = 0, F_0'(0) = 0, \qquad H_0(0) = -nF_0''(0), \qquad G_0(0) = 0, \qquad S_0(0) = \ 0$$

$$F_0(\eta) \to 0\,, H_0(\eta) \to 0\,, G_0(0) \to 0\,, S_0(0) \to 0 \qquad as\ \eta \to \infty \quad (31)$$

As stated by [29], variables $H_0' = 1$ is used in place of the boundary conditions $H_0(\eta) \to 0$ as $\eta \to \infty$ In order to make sure that the least nonzero eigenvalues are produced accordingly.

4. Results and Discussion

In this research work Joule heating and viscous dissipation along with inclined magnetic effects have be discussed numerically for micropolar nanoliquid flow on a nonlinear extending/contracting surface. The governing equations of micropolar nanofluid flow Eq. (8) to Eq. (11) according to the boundary conditions Eq. (12), are numerically elucidated to examine the flow and thermal performance of the liquid. The flow characteristics are examined in graphical form. Table 2 describes the contrast among current results and already published work [30]. The obtained results are showns good agreement with available published work.

Table 1

Contrast of $(C_f(Re_x)^{\frac{1}{2}})$ against K and $n = 0, 0.5$ for $\lambda = 1$, when $\gamma = 1, Sr, D_f, Ec, Rd = 0$.

	$n = 0$		$n = 0.5$	
K	Hayat et al. [30]	Present	Hayat et al. [30]	Present
0	−1.000,00	-1.000,00	−1.000,00	-1.000,00
1	−1.367,870	-1.367,870	−1.224,739	-1.224,739
2	−1.621,222	-1.621,222	−1.414,214	-1.414,214
4	−2.004,129	-2.004,129	−1.732,047	-1.732,047

Triple solutions have been obtained in this research by employing Stability analysis. Eq. (27) to Eq. (30) have a small eigenvalue, which is obtained via bvp4c MATLAB solver. With reference of [31] presents that an unstable flow with an initial change of disturbance is inferred by a negative lowest eigenvalue, whereas a positive smallest eigenvalue express a stable flow with an initial fall of disturbance. Table 2 presents the values of smallest eigenvalue. The first solution is available for positive smallest eigenvalue $(\varepsilon > 0)$, while the second and third solutions are available for negative smallest eigenvalue $(\varepsilon < 0)$. For positive value of ε $(\varepsilon > 0)$, solution is stable while for negative value of ε $(\varepsilon > 0)$, solution is not stable and feasible. Therefore, the decisions taken depend on first solution results. Moreover, there is quiet mathematical importance in the second and third solutions.

Table 2
different values of K and f_w for smallest eigenvalue

		ε		
K	f_w	1st Solution	2nd Solution	3rd Solution
0	3	0.44122	-1.02391	-1.02112
0	2.5	0.36221	-0.66541	-0.65441
0	2	0.01426	-0.10150	-0.10240
1	3	0.36726	-0.75005	-0.64004
1	2.5	0.11161	-0.43401	-0.28570
2	3	0.23073	-0.48260	-0.41260

Figure 2 exhibits the velocity distribution behavior against magnetic field parameter M. The graph presents the velocity distribution for triple solutions for which necessary to fulfill the boundary conditions. The growth of magnetic field strength cause reduction in the velocity distribution in the first solution, the logic behind this behavior is rise in Lorentz force. In view of Lorentz force characteristic it creates high resistance which is the motive behind the decline of momentum boundary layer thickness. Moreover, in the second and third solutions, the velocity distributions shows increasing pattern against the growth of magnetic field's effect.

Figure 3 presents velocity distribution against the variation of n. It is clear from the graph the velocity distribution and boundary layer thickness both improve with the increment in n all 1st, 2nd and 3rd solutions. Physically it happens due to the shear thinning/thickening behavior of the liquid.

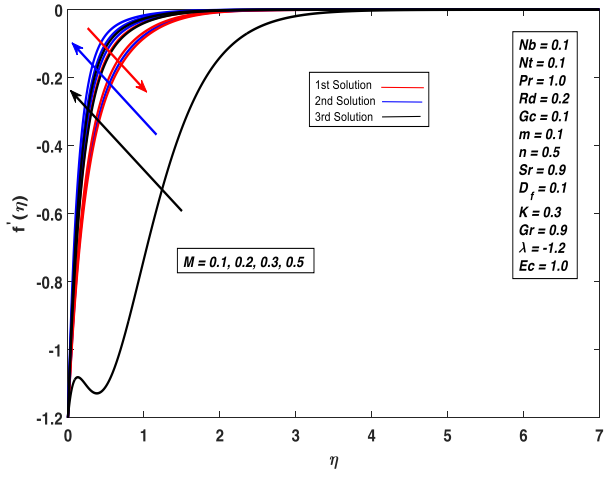

Fig. 2. Velocity profile variations for various M values

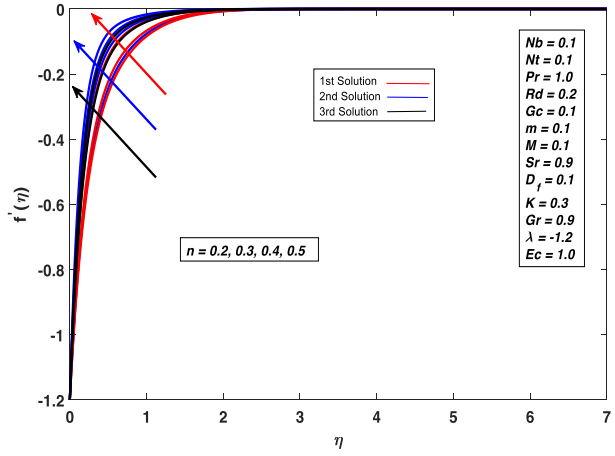

Fig. 3. Velocity profile variations for various n values

Figure 4 exhibits velocity of the liquid against variation of buoyancy parameter Gr. The buoyancy forces help to move fast the fluid flow because the viscous force reduces in this case therefore the fluid velocity graph shows increasing behaviour against the increment of buoyancy factor Gr. The velocity distribution displays increasing pattern in all solutions.

Figure 5 exhibits the influence of material factor K on the microrotation profile. The result presents the boundary layer thickness drop in the case of increasing material parameter value K for the 1st solution while the second and third solutions show increasing behavior with the growth of material parameter K.

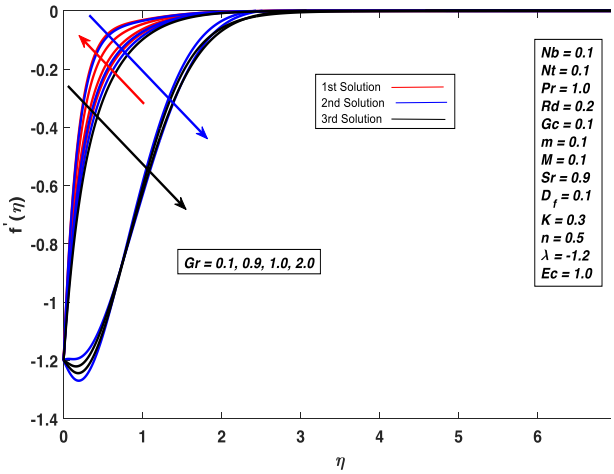

Fig. 4. Velocity profile variations for various Gr values

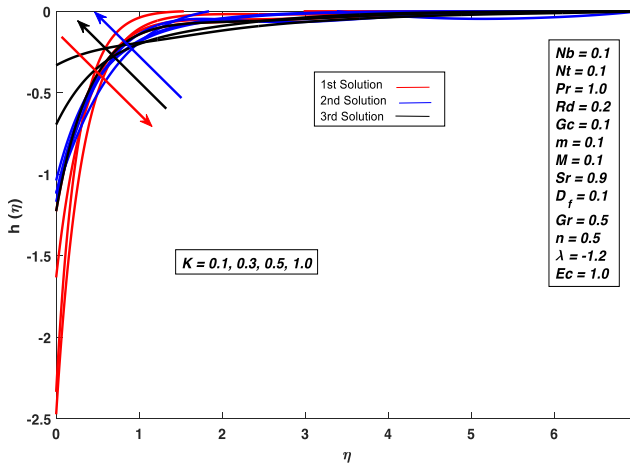

Fig. 5. Microrotation profile variations for various K values

Figure 6 presents the temperature distribution decline for all three solutions with the growth of thermal radiation Rd. The thermal boundary layer and rate of heat transmission both decline in the first, second and third solutions by increasing thermal radiation.

Figure 7 exhibits the effect of Brownian motion factor Nb on temperature distribution. The result express the temperature of the liquid increases with the growth of Brownian motion factor Nb. Logically Brownian motion is an irregular movement of the liquid particles which helps to generate heat which becomes cause of increment in the temperature of the liquid. Finally first, second and third solutions present increment in temperature distribution

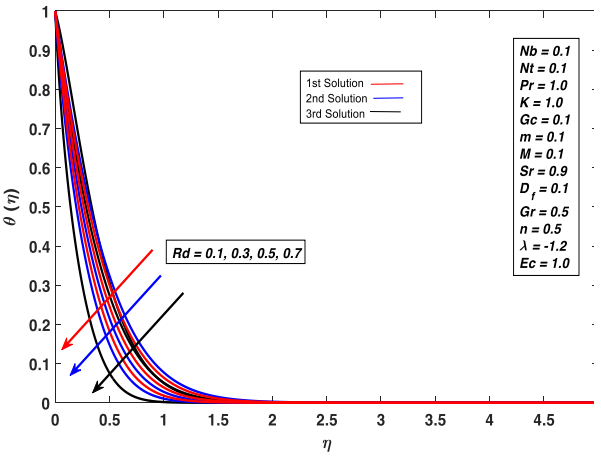

Fig. 6. Temperature profile variations for various Rd values

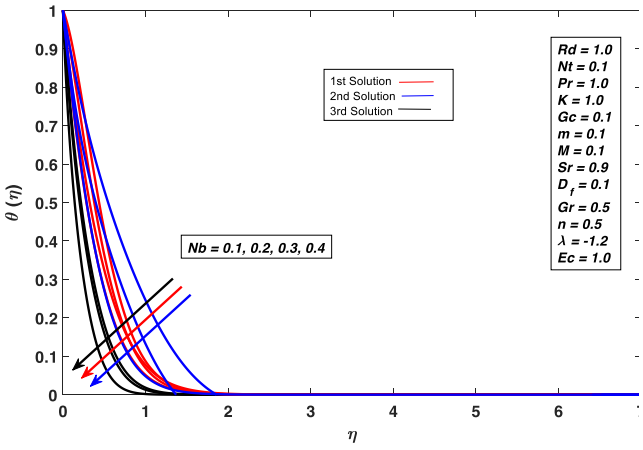

Fig. 7. Temperature profile variations for various Nb values

Figure 8 elucidates the effect of the thermophoresis paramter Nt on temperature distribution. The graphical result illustrates that the thermal boundary layer thickness and the temperature distribution both show increasing behavior against the growth of thermophoresis factor Nt

Figure 9 represents the impact of Eckert number on the temperature distribution. As Eckert number describe the heat dissipation with in the thermal boundary layer. Therore logically by improving Eckert number values the heat dissipation produce with in the thermal boundary lay in return the temperature distribution profile shows increase behavior in all three solutions.

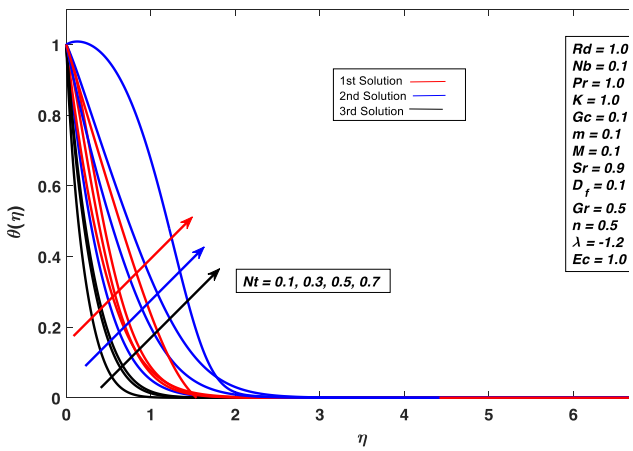

Fig. 8. Temperature profile variations for various Nt values.

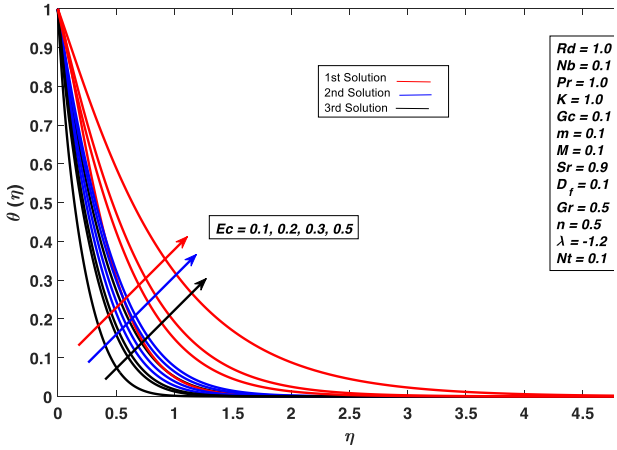

Fig. 9. Temperature profile variations for various Ec values

Figure 10 exhibits Brownian movement of the particles drops the concentration distribution of the flow phenomenon in all three solutions. Logically concentration boundary layer thickness reduces against the increment in the Brownian motion factor Nb. Figure 11 presents the impact of thermophoresis factor on the concentration distribution. The graphical representation shows that the concentration distribution increases for all three solutions because the boundary layer thickness increases for the growth of thermophoresis factor Nt.

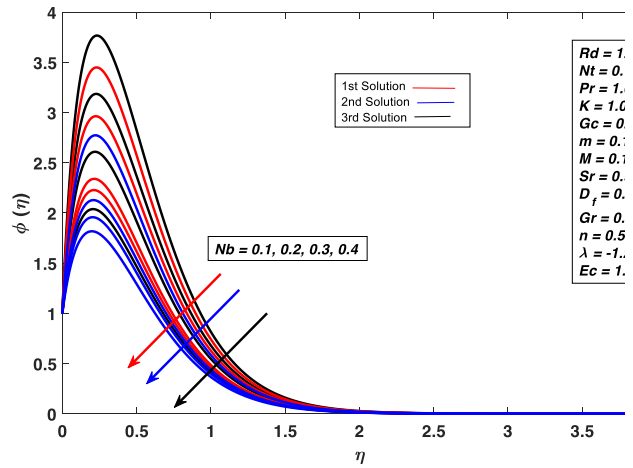

Fig. 10. Concentration profile variations for various Nb values

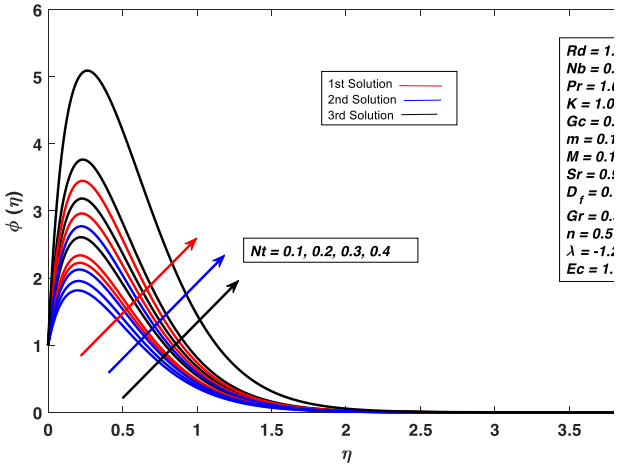

Fig. 11. Concentration profile variations for various Nt values

Figure 12 shows the impact of Dufour factor (Df) on the temperature profile. The temperature distribution contour presents the temperature profile increases in first second and third solution, logically the mass diffusion rate increases. With the increment in mass diffusion-induced, more effective energy transfer. Therefore, with the growth of Df the temperature profile increases. Figure 13 presents the influence of Soret number Sr on concentration distribution. The graph of concentration distribution shows increasing behavior in the first, second and third solutions for the increment in Sr. Physically, the increment in Sr it becomes clear that temperature gradients contribute significantly to species diffusion, which raises concentration.

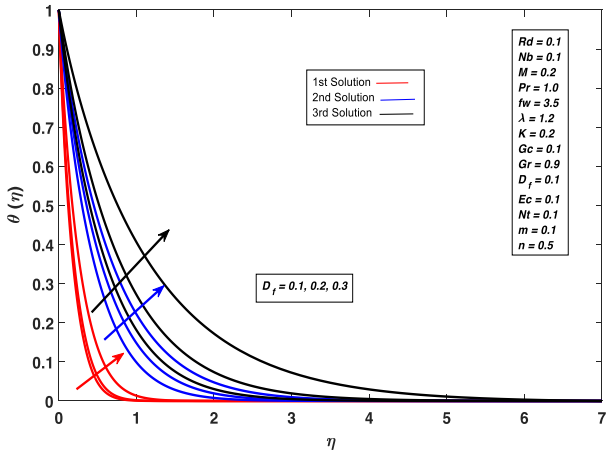

Fig. 12. Temperature profile variations for various Df values

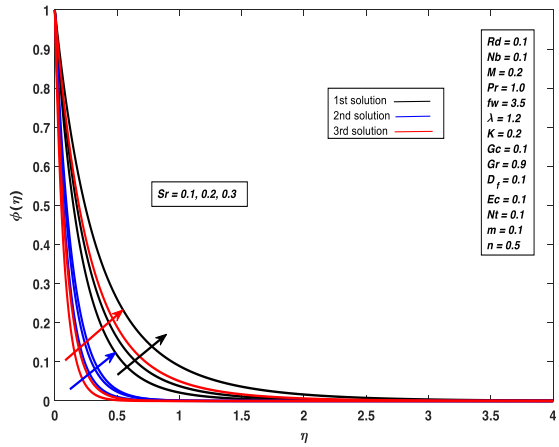

Fig. 13. Concentration profile variations for various Sr values

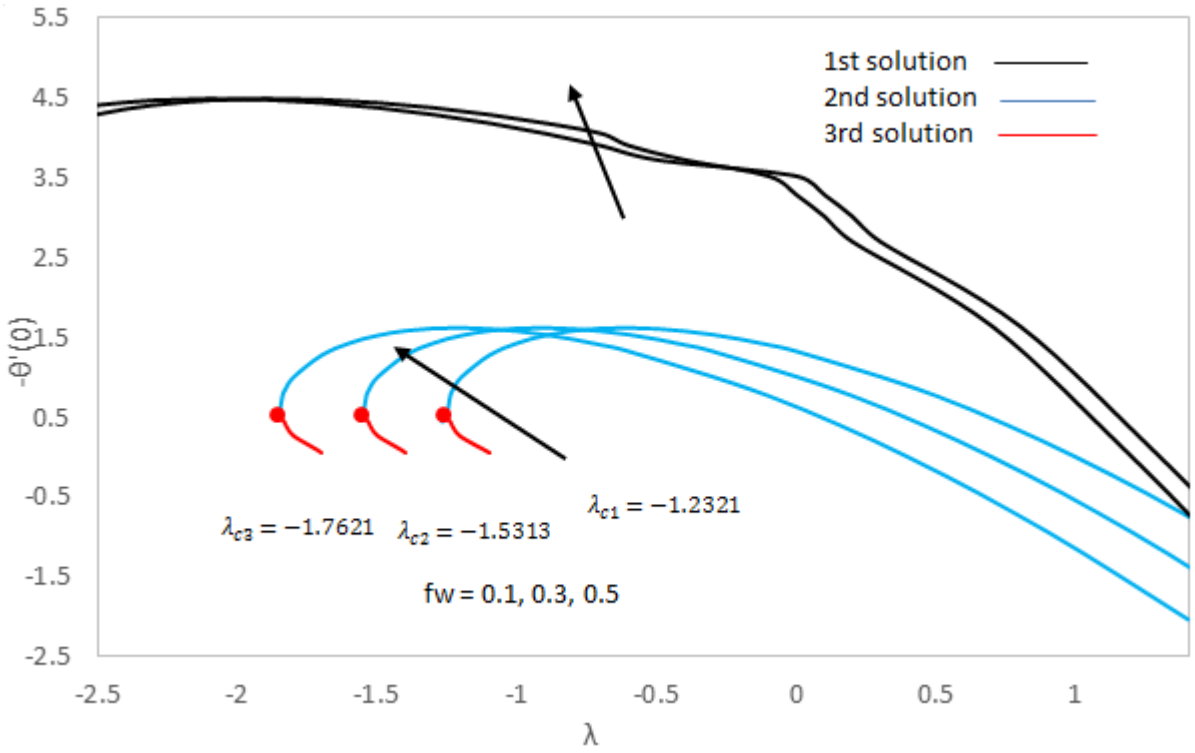

Fig. 14. $-\theta'(0)$ versus λ for different changes in f_w.

Furthermore, figures 14 and 15 shows changes in heat and mass transmission rates against stretching/shrinking factor along with changes in suction factor and magnetic effect. These graphs portray two solutions merges in one another at critical values denoted by $\lambda_{c_1}, \lambda_{c_2}, \lambda_{c_3}$ against changes in suction factor. Figure 14 shows second and third solutions join each other at critical points while first solution move continuously in the same way. Figure 15 portrays mass transmission rate against different values of M. It shows an increasing behavior for changes in suction factor.

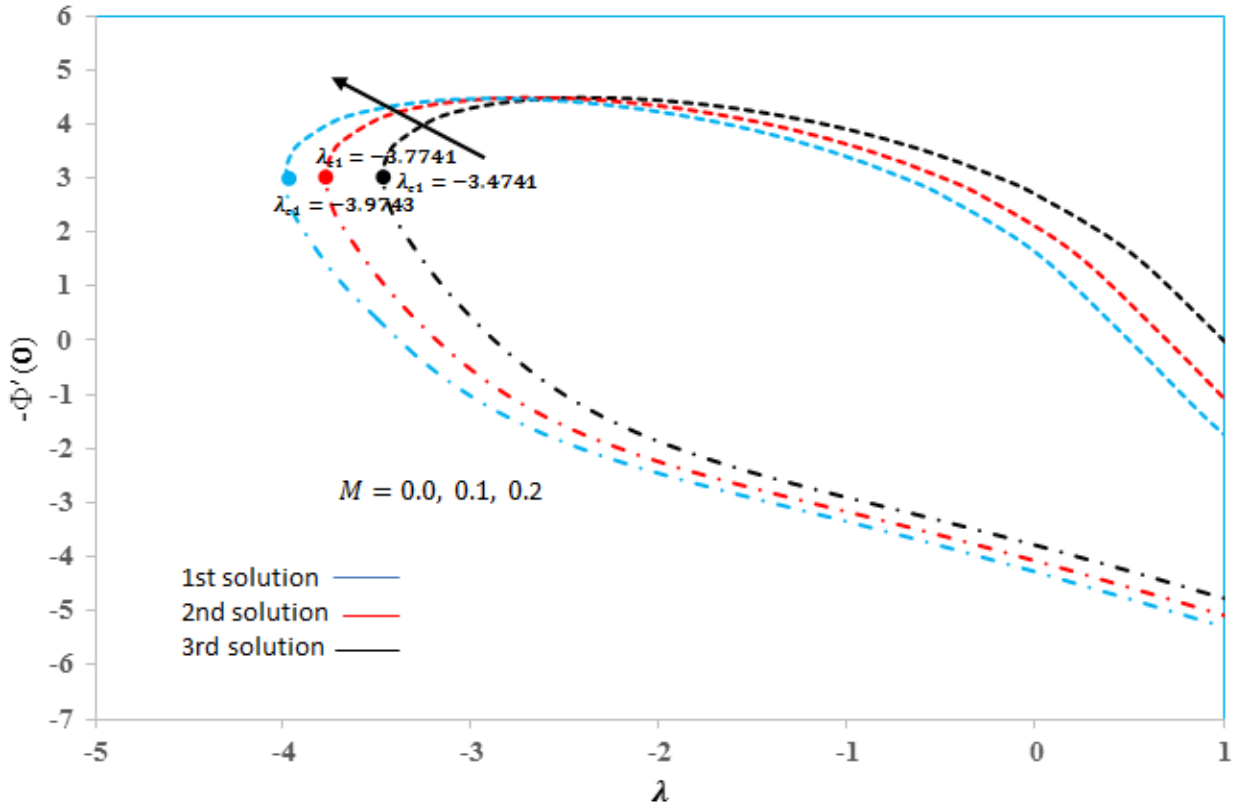

Fig. 15. $-\phi'(0)$ versus λ for different changes in M.

5. Conclusion

In this study triple solutions of the micropolar nanofluid flow were obtained by performing stability analysis. Further Joule heating along with viscous dissipation are taken in account. In addition the stretching/ shrinking surface is porous. Moreover, Soret and Dufour impacts along with inclined magnetic field are considered in the research work. The numerical outcomes were recovered by utilizing bvp4c solver. While for the authenticity of current results a contrast with already published work performed and found a good agreement between results. The main findings of the study under consideration are:

1. The temperature distribution reduces with the growth of thermal radiations.
2. The concentration distribution upsurges by improving N_t.
3. Eckert number improves the temperature distribution of the liquid.
4. Mass transmission rate increases with the increment in magnetic strength.
5. Heat transmission rate increases with the enhancement of suction/injection factor.
6. It is observed first solution is physically stable while remaining two are unstable.

In future this study of micropolar nanofluid flow can be extending for many geometries including, disk, cylinder, sphere, cone and many more.

Acknowledgment
The author extends his appreciation to the Arab Open University for funding this work through AOU research fund No. (AOURG-2025-048).

References

[1] Rafique, K., Kanwal, S., Niazai, S., Alqahtani, A. A., & Khan, I. (2025). Significance of thermal radiation in stability analysis and triple solutions for magnetized micropolar Buongiorno's nanofluid model. *Journal of Radiation Research and Applied Sciences*, *18*(1), 101316.

[2] Rafique, K., Nasim, A., Alshehery, S., Younas, B., Khan, I., & Khan, M. S. (2025). Thermal radiation and stability aanalysis in dual solutions of Al2O3-Cu/H2O hybrid nanofluid flow over a stretching/shrinking surface with arrhenius kinetic energy. *Journal of Radiation Research and Applied Sciences*, *18*(2), 101510.

[3] Choi, S. U., Eastman, J. A. (1995). Enhancing thermal conductivity of fluids with nanoparticles (No. ANL/MSD/CP-84938; CONF-951135-29). Argonne National Lab.(ANL), Argonne, IL (United States). https://www.osti.gov/biblio/196525

[4] Rafique, K., Elkahlout, G., Rehman, A., & Kanwal, S. (2024). Bio convection heat transfer in Sisko nanofluid past a stretching cylinder with Soret and Dufour effects. *Edelweiss Applied Science and Technology*, *8*(6), 5236-5253.

[5] Bouchireb, A., Khan, I., Kezzar, M., Alqahtani, S., Sari, M. R., Rafique, K., & Tabet, I. (2024). MHD Flow of Hybrid Nanofluid Between Convergent/Divergent Channel by Using Daftardar-Jafari Method. *BioNanoScience*, *14*(2), 1583-1600.

[6] Ali, A. R., Rafique, K., Imtiaz, M., Jan, R., Alotaibi, H., Mekawy, I. (2024). Exploring magnetic and thermal effects on MHD bio-viscosity flow at the lower stagnation point of a solid sphere using Keller box technique. Partial Differential Equations in Applied Mathematics, 9, https://doi.org/10.1016/j.pdeapm.2024.100601

[7] Ur Rasheed, H., AL-Zubaidi, A., Islam, S., Saleem, S., Khan, Z., & Khan, W. (2021). Effects of Joule heating and viscous dissipation on magnetohydrodynamic boundary layer flow of Jeffrey nanofluid over a vertically stretching cylinder. *Coatings*, *11*(3), 353.

[8] Lemouedda, B., Kezzar, M., Rafique, K., Sari, M. R., Tabet, I., Khan, I. (2024). Ternary nanoparticles effect in rotating hydromagnetic Jeffery-Hamel flow of nanofluids. Proceedings of the Institution of Mechanical Engineers, Part N: Journal of Nanomaterials, Nanoengineering and Nanosystems, https://doi.org/10.1177/23977914241261514

[9] Wahid, N. S., Mohd Nasir, N. A. A., Arifin, N. M., & Pop, I. (2025). Ternary Hybrid Nanofluid with First and Second Order Velocity Slips: Dual Solutions with Stability Analysis. *Computer Modeling in Engineering & Sciences (CMES)*, *142*(2).

[10] Al Faqih, F. M., Rafique, K., Aslam, S., Swalmeh, M. Z. (2024). Numerical Analysis on Stagnation Point Flow of Micropolar Nanofluid with Thermal Radiations over an Exponentially Stretching Surface. WSEAS Transactions on Fluid Mechanics, 19, 40-48.

[11] Prasad, P. D., Kumar, R. K., Varma, S. V. K. (2018). Heat and mass transfer analysis for the MHD flow of nanofluid with radiation absorption. Ain Shams Engineering J 9(4), 801-813. https://doi.org/10.1016/j.asej.2016.01.013

[12] Sharma, R. P., Mishra, S. R., Tinker, S. (2020). Influence of Soret and Dufour effect on MHD flow over an exponential stretching sheet: A numerical study. Indian Journal of Pure & Applied Physics, 58(7), 558-568.

[13] Rafique, K., Anwar, M. I., Misiran, M., Khan, I., Alharbi, S. O., Thounthong, P., & Nisar, K. S. (2019). Numerical solution of casson nanofluid flow over a non-linear inclined surface with soret and dufour effects by keller-box method. *Frontiers in Physics*, *7*, 139.

[14] Prashanth, M., & Rao, V. S. (2024). The impact of soret, Dufour, and chemical reaction on MHD nanofluid over a stretching sheet. *Partial Differential Equations in Applied Mathematics*, *10*, 100674.

[15] Seid, E., Haile, E., & Walelign, T. (2022). Multiple slip, Soret and Dufour effects in fluid flow near a vertical stretching sheet in the presence of magnetic nanoparticles. *International Journal of Thermofluids*, *13*, 100136.

[16] Pal, D., Mandal, G., Vajravalu, K., (2016). Soret and Dufour effects on MHD convective–radiative heat and mass transfer of nanofluids over a vertical non-linear stretching/shrinking sheet. Applied Mathematics and Computation, 287, 184-200. https://doi.org/10.1016/j.amc.2016.04.037

[17] Raizah, Z., Khan, A., Gul, T., Saeed, A., Bonyah, E., & Galal, A. M. (2023). Coupled Dufour and Soret effects on hybrid nanofluid flow through gyrating channel subject to chemically reactive Arrhenius activation energy. *Journal of Nanomaterials*, *2023*(1), 9208703.

[18] Kumar, M. A., Reddy, Y. D., Goud, B. S., Rao, V. S. (2021). Effects of soret, dufour, hall current and rotation on MHD natural convective heat and mass transfer flow past an accelerated vertical plate through a porous medium. International Journal of Thermofluids, 9. http://dx.doi.org/10.1016/j.ijft.2020.100061

[19] Hussein, U. N., Khashi'ie, N. S., Arifin, N. M., & Pop, I. (2025). Heat Transfer and Flow Dynamics of Ternary Hybrid Nanofluid over a Permeable Disk under Magnetic Field and Joule Heating Effects. *Frontiers in Heat and Mass Transfer*, *23*(2), 383-395.

[20] Hussein, U. N., Khashi'ie, N. S., Hamzah, K. B., Arifin, N. M., & Pop, I. (2024). JOULE HEATING EFFECT ON TERNARY NANOFLUID FLOW AND HEAT TRANSFER OVER A PERMEABLE CYLINDER. *JP Journal of Heat and Mass Transfer*, *37*(6), 831-841.

[21] Rafique, K., Anwar, M. I., Misiran, M., Khan, I., & Sherif, E. S. M. (2019). The implicit Keller Box scheme for combined heat and mass transfer of Brinkman-type micropolar nanofluid with Brownian motion and thermophoretic effect over an inclined surface. *Applied Sciences*, *10*(1), 280.

[22] Yang, H., Hayat, U., Shaiq, S., Shahzad, A., Abbas, T., Naeem, M., ... & Zahid, M. A. (2023). Thermal inspection for viscous dissipation slip flow of hybrid nanofluid (TiO2–Al2O3/C2H6O2) using cylinder, platelet and blade shape features. *Scientific Reports*, *13*(1), 8316.

[23] Naseem, A., & Kasana, A. G. (2024). Numerical assessment of MHD hybrid nanofluid flow over an exponentially stretching surface in the presence of mixed convection and non uniform heat source/sink. *Results in Engineering*, *22*, 102294.

[24] Waini, I., Alabdulhady, S., Ishak, A., & Pop, I. (2023). Viscous dissipation effects on hybrid nanofluid flow over a non-linearly shrinking sheet with power-law velocity. *Heliyon*, *9*(10).

[25] Sademaki, L. J., Reddy, B. P., & Matao, P. M. (2025). Viscous dissipation effects on heat propagating MHD nanofluid flow induced by the Brownian motion and thermophoresis impacts in a vertical cone with convective surface conditions. *Partial Differential Equations in Applied Mathematics*, *13*, 101143.

[26] Aiyashi, M. A., Abo-Dahab, S. M., & Albalwi, M. D. (2023). Effect of viscous dissipation and induced magnetic field on an unsteady mixed convective stagnation point flow of a nonhomogenous nanofluid. *Scientific Reports*, *13*(1), 22529.

[27] Khan, W. A., Pop, I. (2010). Boundary-layer flow of a nanofluid past a stretching sheet. International journal of heat and mass transfer, 53(11-12), 2477-2483. https://doi.org/10.1016/j.ijheatmasstransfer.2010.01.032

[28] Seid, E., Haile, E., Walelign, T. (2022). Multiple slip, Soret and Dufour effects in fluid flow near a vertical stretching sheet in the presence of magnetic nanoparticles. International Journal of Thermofluids, 13, https://doi.org/10.1016/j.ijft.2022.100136

[29] Harris, S. D., Ingham, D. B., Pop, I. (2009). Mixed convection boundary-layer flow near the stagnation point on a vertical surface in a porous medium: Brinkman model with slip. Transport in Porous Media, 77, 267-285. https://doi.org/10.1007/s11242-008-9309-6

[30] Hayat, T., Waqas, M., Alsaedi, A., Khan, M.I. (2017). Radiative flow of micropolar nanofluid accounting thermophoresis and Brownian moment. Internation Journal of Hydrogen Energy, 42, 16821–16833. https://doi.org/10.1016/j.ijhydene.2017.05.006

[31] Lund, L.A.; Omar, Z.; Khan, I. (2019). Quadruple solutions of mixed convection flow of magnetohydro- dynamic nanofluid over exponentially vertical shrinking and stretching surfaces: Stability analysis. Computer. Methods and Programs in Biomedicine, 182, https://doi.org/10.1016/j.cmpb.2019.105044